Growth below and above the spinodal limit: The cholesteric-nematic front

P. Oswald, J. Baudry,* and T. Rondepierre
Laboratoire de Physique de I'Ecole Normale Supérieure de Lyon, UMR 5672 du CNRS, 46 Allée d'Italie, 69364 Lyon Cedex 07, France

(Received 9 December 2003; revised manuscript received 13 February 2004; published 19 October 2004)

In classical crystal growth, the solid propagates into its metastable liquid, even in the fast-dynamics regime in which kinetic effects dominate the diffusive effects. In usual experiments, the liquid is always very far from its spinodal limit below which it becomes unstable. For that reason, very little is known about crystal growth just below and above the spinodal limit of the liquid. In order to tackle this problem, we have performed an experiment about the propagation of the cholesteric-nematic front in directional melting. We show experimentally that, in this system, it is possible to reach and pass the spinodal limit. We show the existence of many morphological transitions at increasing velocities which lead to the formation of metastable or unstable phases. A complete phase diagram is drawn up as a function of the front velocity and the sample thickness. In particular, the crossing of the spinodal limit is clearly identified by comparison with the morphologies observed in free growth (i.e., at a homogeneous temperature). We show that this passage is accompanied by a reversal (π rotation) of the structure in thin samples only. This spectacular effect resembles a "cell-to-dendrite" transition and is chirality induced. The importance of the first-order character of the transition is also emphasized.

DOI: 10.1103/PhysRevE.70.041702 PACS number(s): 61.30.Jf, 83.80.Xz, 82.60.Nh, 68.35.Md

I. INTRODUCTION

The growth of a solid from a liquid (or a vapor) phase has been studied for a long time. It leads to different morphologies which strongly depend on experimental conditions. The best-known example is that of the snowflakes, which form a vast number of branched structures named dendrites [1]. All these morphologies are, by nature, out of equilibium, and form a subclass of the more general problem of pattern formation in dissipative systems. Indeed, very similar problems are met in hydrodynamics (Rayleigh-Bénard convection [2] and Taylor vortices [3]), superconductors [4], dielectric breakdown fronts [5], etc.

In usual crystal growth, the ordered phase (the solid) is growing into the disordered phase (the liquid). In most experiments, the liquid is metastable and the crystal front morphology results from a competition between the diffusion of heat (or of impurities) and the surface tension or kinetic effects (Mullins-Sekerka instability [6]). On the other hand, the structure of the crystal remains mainly unchanged during the growth process.

The situation becomes different if the growth is very fast. In that case, attachment kinetic effects dominate all the physics, and impurity diffusion becomes negligible (at very large velocity, impurities are trapped by the solid because they have no more time to diffuse). The stucture of the solid can also change, an effect which becomes more important as the liquid approaches its spinodal limit. In particular, metastable phases can nucleate and develop [7], either because the nucleation rate of the metastable phase exceeds that of the stable phase, or the growth velocity of the former is larger than that of the latter [8]. Another possibility is that the front splits into two fronts — one between the disordered and the metastable phases and another between the metastable and the stable phases [9]. The metastable phase can then develop if the first front moves faster than the other. Finally the solid can be trapped in an amorphous state if it is quenched very fast below the spinodal limit of the liquid (typical critical cooling rate for obtaining a glass is 10^6 K/s). In that case, front propagates into an unstable state [10,11]. Note that the propagation of a front in such a case has only been addressed experimentally when the phase transition is second order (for instance, in hydrodynamics [2,3]).

Of course, the main difficulty of studying the fast dynamics of fronts in crystals is that their velocities are extremely large (m/s or much more), rendering almost impossible their observation. Another difficulty is to quench the system very quickly (in less than one ms or even much less) over a large interval of temperature (tens of degrees) in a controlled way.

In this paper, we propose to tackle the general problem of front propagation below and above the spinodal limit in liquid crystals. These materials already turned out to be very interesting to study Mullins-Sekerka instability [12–14]. In particular, they allowed the discovery of many secondary instabilities of cellular fronts [13–16] which have then been observed in many other systems (eutectics, in particular [13]). We show in the following that they can also be used for studying fast dynamics of fronts propagating into a metastable or a unstable liquid.

The front chosen is the cholesteric-nematic front. Before explaining how it is prepared, let us emphasize that the cholesteric phase will play the role of the "solid" and the nematic, that of the "liquid." The main advantage of this system, in comparison to usual crystals, is that their periodicity develops at a mesoscopic scale, in the range of micrometers, instead of nanometers. From this point of view, a cholesteric resembles a colloidal crystal. For that reason, kinetic effects are much slower than in usual solids, which allows us to

*Permanent address: Laboratoire Colloïdes et Matériaux Divisés, ESPCI et CNRS UMR 7612, 10 rue Vauquelin, 75231 Paris Cedex 05, France.

reach very easily the spinodal limit of the "liquid."

We now recall the basics about the cholesteric-nematic phase transition. A cholesteric phase is a nematic liquid crystal that is twisted in a single direction. Although the cholesteric and the nematic phases are not thermodynamically distinct, it is possible to induce the cholesteric-nematic transformation by subjecting the cholesteric to an electric field or a topological frustration. This transition is subcritical, i.e., first order (in contrast with usual Frederiks transitions in nematics, which are usually second order), which leads to a great variety of patterns. These include "fingers" of different types (four, at least) — inversion walls, spherulites, and transient unstable patterns. For this reason, it has attracted much attention, from both experimentalists [17–19] and theorists [20–23]. Note that Refs. [17–23] only concern continuous fingers of the first kind, which we will only consider in the following (for a general review, see Ref. [14], Vol. 1, Chap. VII, and Ref. [24]).

One usual way to observe this transition is to confine the cholesteric between two glass plates treated to give homeotropic anchoring. This surface treatment imposes a perpendicular boundary condition on the rodlike molecules. This boundary condition is topologically incompatible with the helical structure of the cholesteric phase and can lead to its complete unwinding, giving a homeotropic nematic phase [14,17–24]. The control parameter of this transition is the confinement ratio $C=d/p$, where d is the sample thickness and p is the equilibrium pitch of the bulk cholesteric phase: when $C<C_c$, the nematic phase occurs; whereas the cholesteric phase develops when $C>C_c$. In practice, C_c is always of order unity, even if it depends on the values of the Frank constants K_i $(i=1,2,3)$. In the present experiment, the liquid crystal is a mixture of 8CB (4-*n*-octyl-4′-cyanobiphenyl from Merck Ltd.) to which 0.45% of the chiral molecule S811 (from Merck Ltd.) has been added. In an infinite medium, this mixture has a cholesteric–smectic-*A* transition at temperature $T_{A\mathrm{Ch}}$. It turns out that the pitch of the cholesteric phase diverges when the temperature approaches $T_{A\mathrm{Ch}}$. As a consequence, for each homeotropic sample of finite thickness, there is an interval of temperature $[T_{A\mathrm{Ch}},T_c]$ in which the nematic phase is stable. Note that T_c is given by the relation $d/p(T_c)=C_c(T_c)\approx 1$. Thus, thicker samples produce a more narrow temperature interval. Because this interval always exists, one systematic way to observe the nematic-cholesteric phase transition is to progressively increase the temperature of the sample from the smectic phase. The only condition to fulfill in that case is that the sample thickness should be large enough for the cholesteric phase to develop before the liquid crystal melts. Such an experiment is called a free-growth experiment.

Another way to observe the transition is to use directional melting. The sample is placed in a temperature gradient. This way, the smectic phase occurs at the cold side of the sample, whereas the cholesteric phase develops at the hot side. In between, a nematic band forms.

In this article, we study cholesteric-nematic fronts where the sample is moving at constant velocity V towards the hot side (directional melting of the smectic phase). This geometry was first explored in 1987 [25], where different patterns were seen to develop behind the moving cholesteric–smectic-*A* front, depending on velocity and sample thickness. More precisely, it was observed that at rest and at small velocities, the cholesteric phase consists of bands that are perpendicular to the moving interface. It was shown later that these bands are cholesteric fingers of the first kind (CF-1, for which the director field is continuous everywhere) with their rounded tips [18,19] at the interface (regime 1). At larger velocities, the fingers directly form parallel to the interface (regime 2). At still higher velocities, the fingers are replaced by a uniform gray region corresponding to a translationally invariant configuration (TIC) in which the helical axis is perpendicular to the glass plates [19]. This region is followed by a square lattice of doubly periodic fingers (regime 3) or by fingers that are more or less perpendicular to the interface but have many edge dislocations (regime 4). These four regimes do not systematically develop at all thicknesses as shown by the direct observation of patterns in a sample of variable thickness along a direction perpendicular to the thermal gradient [25]. In particular, it was shown that regimes 2 and 3 only develop in samples of intermediate thicknesses (when the value of C measured close to T_{ChI} typically ranges between 1.25 and 1, where T_{ChI} is the cholesteric-isotropic transition temperature).

More recently, we observed that in very thin samples (i.e., with smaller values of C than in the samples used in Ref. [25]) another pattern develops, consisting of CF1 with their pointed tips at the interface. This observation was briefly mentioned in Refs. [14,24].

Our goal is to collect all these observations and, more importantly, to establish a relationship between the morphologies observed at the front in directional melting and those observed in free growth, at the same temperature. The idea behind this comparison is to determine which (if any) of the morphological transitions observed at increasing velocities can be attributed to the passage by the spinodal limit of the nematic phase, where the energy barrier goes to zero (as we know that the cholesteric-nematic transition is first order because of the elastic anisotropy of the elastic constants [25]). Another point is to look for metastable phases, as we know from theory [8,9] and experiments in solids [7] that they can sometimes develop at large supersaturation.

The plan of the article is the following. In Sec. II, we briefly describe the experimental setups, and in Sec. III we describe the experimental procedures used to identify the different regimes. In Sec. IV, we compare the morphologies observed in directional melting with those observed at the same temperature in free growth. In this way, we clearly identify the formation of two metastable phases and the change of morphology at the passage of the spinodal limit, i.e., when the nematic phase, first metastable, becomes unstable. Our results are summarized in Sec. V where we draw up the experimental phase diagram, and then discussed from a topological point of view in Sec. VI. The role of the first-order character of the cholesteric-nematic transition on the nature of the observed bifurcations is underlined in Sec. VII. Conclusions are given in Sec. VIII.

II. EXPERIMENTAL APPARATUS

The samples are prepared between two parallel glass plates (5 cm $\times$ 2.5 cm in size and 1 mm thick) covered by a

transparent ITO layer which allows us to apply an electric field to the sample. The liquid crystal (8CB+0.45% S811 in weight) is of positive dielectric anisotropy. So, imposing an electric field favors the nematic phase. The homeotropic anchoring (molecules perpendicular to the surfaces) is obtained by depositing on the two electrodes with a spin coater a thin layer of polyimide 0626 from Nissan (diluted to 3% in weight in solvent 26 from Nissan). This layer is then polymerized in two steps—15 mn at 90 °C and 1 h at 180 °C. This surface treatment gives a very strong homeotropic anchoring, which can be considered as "infinite." The two plates are separated by wire spacers, with typical thicknesses 15–70 μm.

The cell for directional melting experiments has been described in detail in [27]. It contains two ovens whose temperatures are individually controlled. The ovens are separated by a gap of 4 mm and the sample straddles the space between them. The temperatures are chosen in order that the two fronts — cholesteric-nematic and nematic–smectic-*A* — are visible under the optical microscope. The temperature gradient was determined with a dummy cell with a thermocouple and by measuring the temperature at different points in the gap between the two ovens. A stepping motor allows us to move the sample in both directions in the temperature gradient at a controlled velocity.

For free-growth experiment at a controlled temperature we used an oven regulated within ±0.01 °C. This oven was mounted on the stage of a polarizing microscope and allowed us to observe the nucleation and the growth of the cholesteric phase into the nematic one. An ac electric field can be applied to the sample to unwind transiently the cholesteric phase into the homeotropic nematic phase. It must be applied during a very short time (1 s, typically) to not heat the sample and change its temperature. All observations are done under the microscope using crossed polarizers.

The equilibrium pitch p of the cholesteric phase has been measured by using the Cano-Grandjean wedge technique in the range of temperature (34–40 °C) [26]. The data are very well fitted to the following function $p=a+bT+c/(T-T_{chA})^{\nu}$, where T is given in degrees Celsius, with $a=16\pm0.37$, $b=-0.054\pm1.7$, $c=5.94\pm0.11$, and $\nu=1.92\pm0.3$. These measurements show that $p\approx14$ μm at the transition temperature towards the isotropic liquid ($T_{ChI}\approx41$ °C) and changes very little between T_{ChI} and $T_{ChI}+4$ °C. On the contrary, p diverges when $T\rightarrow T_{ChA}$, with $T_{ChA}=33.08\pm0.02$ °C. This is due to the fact that the twist constant K_2 diverges as the temperature tends to T_{ChA} [14].

III. EXPERIMENTAL PROCEDURE

For each sample thickness, we observed the structure of the cholesteric-nematic front in the microscope as a function of the pulling velocity. When the permanent regime was reached, we determined the temperature T_f of the front from the measurement of the width W of the nematic band by using the relation

$$T_f = T_{ChA} + GW,$$

where G is the temperature gradient (constant within the nematic band) and T_{ChA} the temperature of the cholesteric (nematic)–smectic-*A* front (also constant within a few mK as kinetics at this interface have been shown to be very fast [28]). As we explained above, G can be easily measured with a thermocouple. By contrast, W is more difficult to determine as the nematic–smectic-*A* front is almost invisible in the microscope between crossed polarizers (both phases are dark in these conditions). A trick (already used by Yethiraj and Bechhoefer [29]) to visualize this front is to use the fact that the nematic phase fluctuates much more than the smectic one. So subtracting two images taken at a short interval of time (typically 0.1 s) allows us to clearly see the front in the microscope. As for the cholesteric-nematic front, it is easily visible between crossed polarizers because of the birefringence of the cholesteric phase. In that way, it was possible to detect the positions of the two fronts and to measure W accurately (usually within ±0.02 K).

In order to answer the question about the stability of the nematic phase ahead of the front at temperature T_f, we observed in the same sample the growth of cholesteric germs in the nematic phase at the same temperature T_f in the absence of a temperature gradient (free-growth experiment). In that way, it was immediately possible to decide whether the nematic phase was stable or metastable.

We emphasize that the structure of the fronts observed in free growth and in directional growth are identical provided that their temperatures are the same and the nematic phase is metastable. That means that the temperature gradient does not modify the inner structure of the front (as shown theoretically in [11], when the thermal length is much larger than the front width, of the same order of magnitude as the sample thickness).

IV. EXPERIMENTAL RESULTS

We have already emphasized in the introduction that the front morphologies observed at increasing velocities strongly depend on the sample thickness d (or, equivalently, on the ratio $C=d/p$, where p is the value of the pitch measured at high temperature, close to the isotropic phase, in our mixture $p=14$ μm). For this reason, we shall distinguish three types of samples: the thin ones ($C<1.8$ or $d<25$ μm), the ones of intermediate thicknesses ($1.8<C<2.5$ or 25 μm$<d<35$ μm) and the thick ones ($C>2.5$ or $d>35$ μm). For each category of samples, we shall describe the front morphology and give its temperature as a function of its velocity. These results will then be compared to the pattern observed in free growth at similar temperatures. In all experiments, the temperature gradient was fixed to $G=16.4$ °C/cm (our results are independent of G in the whole range of G accessible experimentally). For the sake of clarity, we shall first describe our results in thin and thick samples, in which observations are very clear. Then we shall describe an example of a sample of intermediate thickness, which has a more complex behavior. Our observations will be then collected in a bifurcation diagram given in Sec. V.

A. Thin samples ($d<25$ μm)

In Fig. 1 we show a sequence of pictures of the front taken at different velocities in a sample of thickness

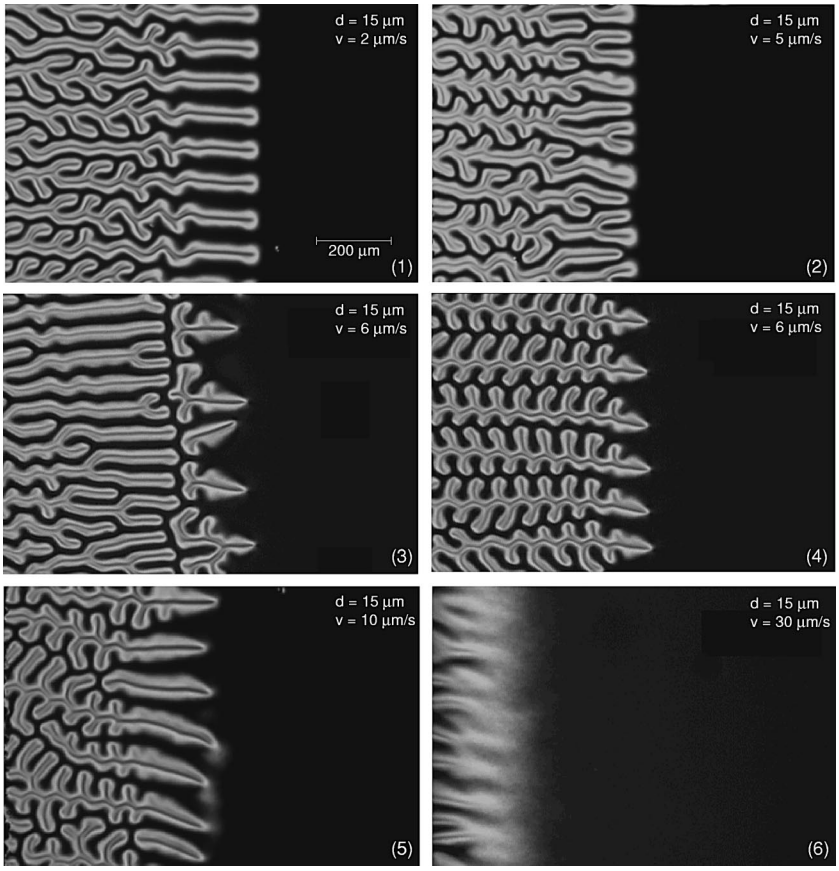

FIG. 1. Different patterns and interfaces observed in directional melting as the velocity was varied ($d=15$ μm).

$d=15\pm1$ μm. At very small velocities ($v<v_-=2.5$ μm/s) the fingers (CF1) are perpendicular to the front with their rounded tips at the front. They are separated from each other by a large band of nematic phase. We note in Fig. 1(1) that the fingers develop side branches at some distance of the front. At this place, the temperature is larger by about 0.3 °C than that of the front. As we shall see later, T_- is the temperature below which isolated fingers can grow in free growth [Fig. 3(1)], whereas above T^- the rounded tip of the finger splits continuously to give a "flowerlike" growth mode, with the pointed tip growing separately [Fig. 3(2)].

The front morphology does not change significantly between $v_-=2.5$ μm/s and $v_j=6$ μm/s [Fig. 1(2)]. The main change is that the fingers easily split at their tips which are always of the rounded type. We can note from now on that at the corresponding temperature of the front T_-, the growth mode observed in free growth is of the flowerlike type. This regime, as the previous one, will be called the "cellular" regime in the following (in comparison with what happens in directional solidification of solids).

A drastic modification of the front occurs at $v_j=6$ μm/s [Fig. 1(3)]. Indeed the present front can no longer propagate at the imposed velocity. As a result, its temperature starts to gradually increase (the front moves to the left on the picture), leaving a band of nematic completely unstable in front of the interface. This band rapidly develops a TIC structure which simultaneously modulates to give new fingers with their "pointed" tips at the front. After a long transient, a new morphology develops, consisting of fingers (CF1) perpendicular to the front, but with their pointed tips at the front [Fig. 1(4)]. Because the tips are strongly spaced, side branches (which are new fingers ended by rounded tips) rapidly develop behind the front to fill the space between the primary fingers. This regime (which we call improperly the "dendritic" regime because of the resemblance between the fingers and real dendrites in crystalline growth) is stable over a large range of velocities (typically between $v_j=6$ μm/s and $v^*\approx25$ μm/s). It is crucial to note that in this regime the tips of the "dendrites" are colder than the tips of the cells observed in the previous regime (see below).

At larger velocities ($v>v^*\approx25$ μm/s), the fingers disappear at the front and are replaced by the TIC. It must be noted that this transition is progressive and much less clear than the previous one. Indeed, the fingers are more and more squeezed between each other in the dendritic regime [see, for instance, Fig. 1(5)] till their spatial periodicity disappears. Note that the fingers reappear behind the front (by forming numerous dislocations) in the TIC regime [Fig. 1(6)].

These different regimes are clearly visible on the curve of temperature of the front as a function of the velocity [Fig. 2(a)]. The linear part of the curve at small velocities ($0<v<v_j$) correspond to the "cellular" regime. The "cell-to-dendrite" transition at v_j is marked by a jump in the curve from temperature T^* to some lower temperature T_j. In the dendritic regime ($v_j<v<v^*$), the front temperature increases rapidly from T_j to T^* and then saturates (within the precision of our measurements) at temperature T^*. At point (v^*,T^*), the TIC solution is fully developed at the front. This point is not clearly defined due to the fact that the

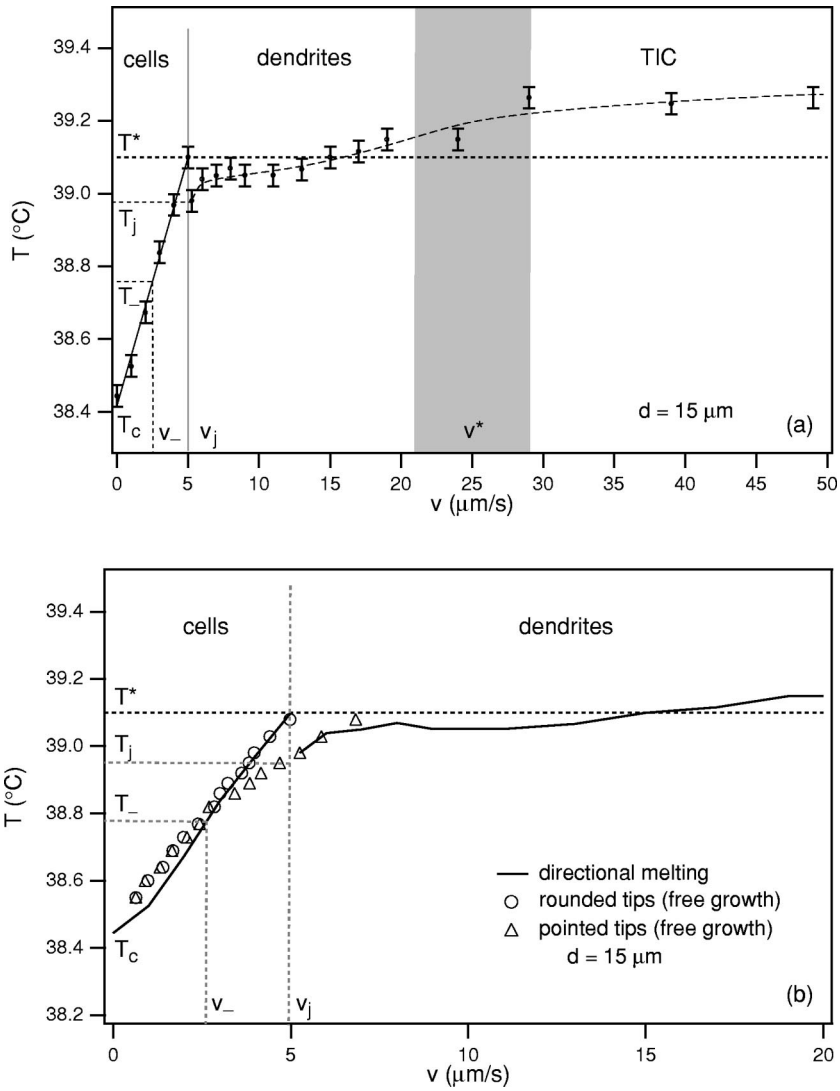

FIG. 2. (a) Front temperature as a function of velocity. The line in the "cellular" regime is the best fit to a linear law of the experimental data. The dashed line in the dendritic and TIC regimes is just a guide for the eyes; (b) superimposition of the data "temperature versus velocity" obtained in directional melting and in free growth. The solid line corresponds to the data obtained in directional melting. The triangles (rounded tips) and the circles (pointed tips) correspond to the data obtained in free growth ($d=15\ \mu$m).

transformation from dendrite to TIC is progressive (the large gray vertical band centered on v^* in the graph of Fig. 2 underlies this point). Above v^*, the width of the TIC band and the front temperature continuously increase. Note that the front temperature tends to saturate at very large velocity.

To complete these observations we looked at the front morphologies in free growth. As expected, we observed isolated fingers growing in the metastable nematic phase from their two tips between T_c and T_- [Fig. 3(1)]. Between T_- and T^*, the rounded tip of the finger splits continuously in time, whereas its pointed tip remains unchanged: the nematic is still metastable [Fig. 3(2)]. A very interesting observation (which escaped us before) is that the two tips propagate at the same velocity between T_c and T_-, whereas the pointed tip moves faster than the other between T_- and T^* (Fig. 4). Finally, the nematic is completely unstable above T^* and develops a TIC structure, which subsequently slowly modulates to give fingers with a large number of dislocations (Fig. 5).

In Fig. 2(b), we superimposed the curves of temperature obtained in directional melting and in free growth. As expected, they perfectly coincide in the cellular regime (between T_c and T^*) and in the dendritic regime (between T_j and T^*).

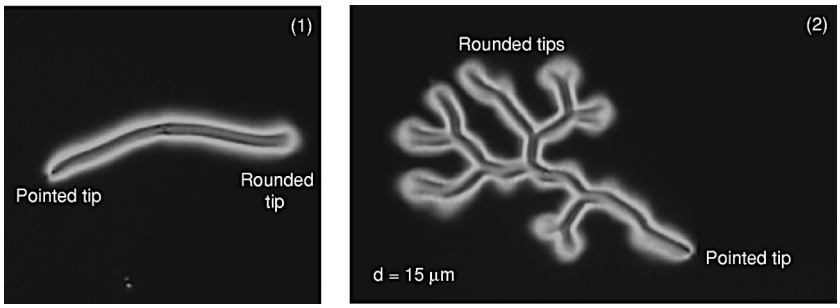

FIG. 3. Isolated fingers (1) and a "flowerlike" pattern (2) observed in free growth at $T=38.55$ and 38.92 °C, respectively ($d=15\ \mu$m).

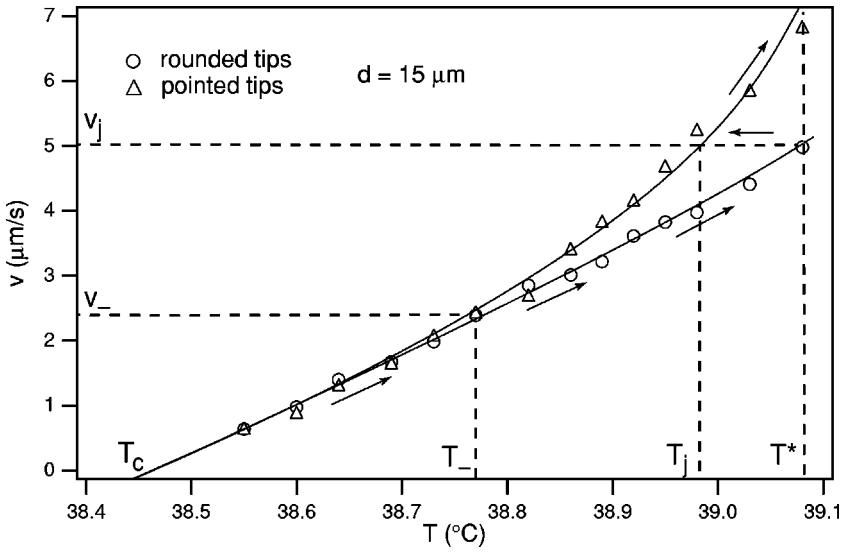

FIG. 4. Velocities of the rounded and of the pointed tips of the fingers. Between T_c and T_-, the cholesteric domain is an isolated finger [Fig. 3(1)]; between T_- and T^*, the cholesteric domain is of the flowerlike type [Fig. 3(2)]. The solid lines are just guides for the eyes. The arrows show the type of solution chosen in directional melting at increasing velocity. The "cell-to-dendrite" transition occurs at velocity v_j ($d=15$ μm).

From these observations we conclude that T^* corresponds to the temperature above which the nematic phase becomes completely unstable (spinodal limit of the nematic phase). The "cell-to-dendrite" transition, as well as the "dendrite-to-TIC" transition occur in directional melting at T^*, i.e., when the nematic phase ahead of the front becomes unstable. Finally, the front chooses in directional melting between v_- and v_j the cellular solution (instead of the dendritic solution which could also exist in this interval of velocities). This allows the system to minimize the width of the nematic band (and so its global supersaturation). Between v_j and v^* the only solution is the dendritic one, which, consequently, is selected. In this regime (as in the previous one) the nematic ahead of the interface is metastable (close to v_j) and at the limit of stability when the velocity approaches v^*. Finally, the TIC clearly develops at the front when any of the previous solutions can no longer propagate at the imposed velocity. In that case, the cholesteric phase grows into the unstable nematic phase and the interface becomes very diffuse with a temperature that slowly increases when the velocity increases.

B. Thick samples ($d>35$ μm)

In thick samples, our observations in directional melting are similar to those done 15 years ago [25]. Figure 6 recalls a typical sequence of the different patterns observed at increasing velocities in a 40 μm-thick sample ($C=2.86$). At small velocity ($v<v_{\parallel}\approx 7$ μm/s), the fingers (CF1) are perpendicular to the front, with their rounded tips at the front ["cell" regime, Fig. 6(1)]. At $v_{\parallel}$, the fingers abruptly rotate about 90° to lie parallel to the front. This morphology [Fig. 6(2)] is observed in a small range of velocities, till velocity $v_{\square}\approx 9$ μm/s.

At $v_{\square}$ a narrow band of TIC occurs at the front. This solution is unstable and relaxes to a periodic state of lower energy. What this periodic state looks like depends on the velocity. Between $v_{\square}$ and $v^*\approx 13$ μm/s, we observe a square lattice, whereas above v^* the TIC gives fingers perpendicular to the front with many dislocations. In this last regime the width of the nematic band strongly increases.

One observation not mentioned in Ref. [25] is that the fingers parallel to the front as well as the square pattern

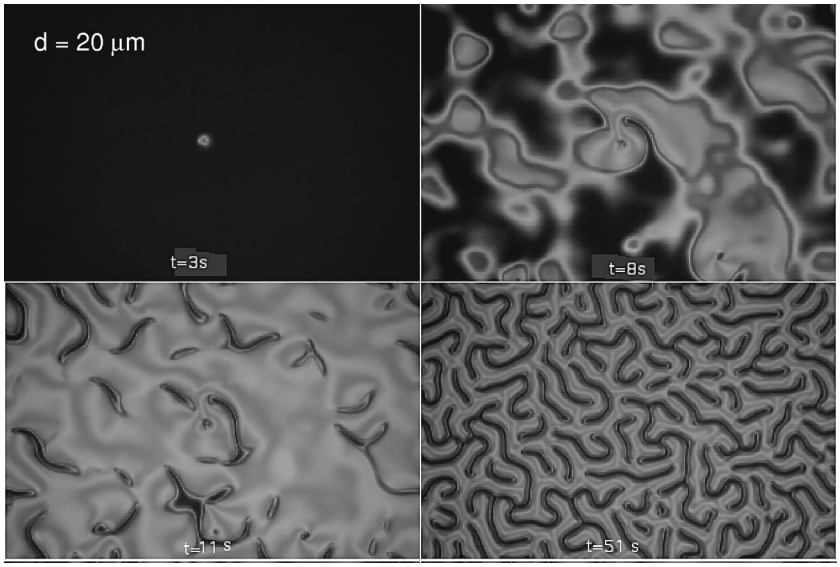

FIG. 5. Destabilization of the nematic phase in free growth above T^* ($T=33.35$ °C, $d=20$ μm).

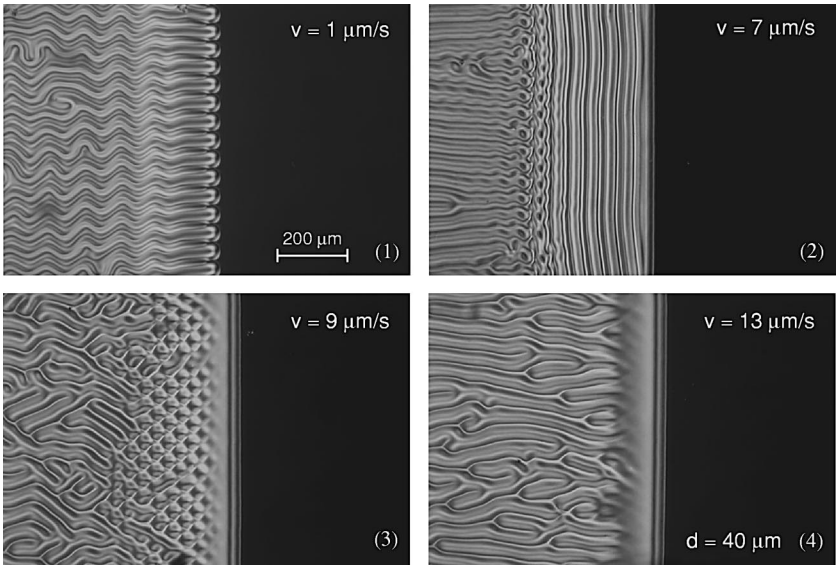

FIG. 6. Different patterns and interfaces observed in directional melting as the velocity was varied ($d=40$ μm). Note that the parallel fingers and the square pattern both transform into fingers perpendicular to the front at some distance from the latter. This defines two secondary interfaces propagating at the same velocity as the front.

certainly form *metastable structures*. Indeed, they systematically transform into fingers perpendicular to the front at some distance from it. This is particularly well visible in Fig. 6(2) where a new interface separating two regions with fingers oriented to 90° from each other propagates at the same velocity as the front.

The question that now arises (and which was not addressed in Ref. [25]) is at which velocity the nematic phase ahead of the front becomes unstable? To answer this question, we measured the front temperature as a function of the velocity. Our measurements are reported in Fig. 7(a). The first observation is that kinetics are almost linear (within experimental errors) till $v_{\square}$ (at this velocity the front temperature equals $T_{\square}$). The second observation is that the front temperature increases more slowly between $v_{\square}$ and v^* (corresponding to temperature T^*). This effect becomes much more pronounced above v^*, where the front temperature tends to strongly saturate: this result suggests that the spinodal limit is reached at v^*.

To confirm these expectations, we observed the front morphologies in free growth at different temperatures. We observed that between T_c and T^* the nematic phase is metastable, whereas above T^* the nematic phase is completely unstable. In addition, we observed the same patterns in free growth as in directional melting, provided that the front temperatures are the same. This is clearly visible in Fig. 8 (to be compared to Fig. 6). Finally, we superimposed in Fig. 7(a) the curves of temperature obtained in directional melting and in free growth. As expected, they coincide in the three regimes observed between T_c and T^*.

The same sequence of morphological transitions was observed in all the samples of thickness lying between 35 and 45 μm. Between 45 and 50 μm, the square pattern disappears while at thicknesses larger than 50 μm, parallel fingers and square pattern both disappear; in that case, the fingers with their rounded tips at the front transform directly and continuously into the TIC solution. We checked again that the TIC is fully developed at velocity v^* corresponding to temperature T^* measured in free growth. The curves "temperature versus velocity" obtained in directional melting and in free growth in a 50 μm-thick sample are shown in Fig. 7(b). They perfectly concide till T^*. Note also that, again, the front temperature increases more slowly above v^* than below, where kinetics are linear within experimental precision. The situation is more complicated at intermediate thicknesses (25 μm$<d<35$ μm). In the following we show what happens at $d=33$ μm.

C. An example of a sample of intermediate thickness ($d=33$ μm)

In this case the sequence of morphological transitions observed in directional melting is richer than in thin samples because parallel fingers form between the "cells" and the "dendrites."So the complete sequence observed at increasing velocity is the following: cell, parallel fingers, dendrites, and TIC. As before, it can be checked that the spinodal temperature T^* is reached two times when the parallel fingers transform into dendrites and when the dendrites transform into TIC. This is clearly visible in the graph of "temperature versus velocity" in Fig. 7(c).

In the next section, we draw up the experimental bifurcation diagram.

V. BIFURCATION DIAGRAM

Our results are summarized in the bifurcation diagram of Fig. 9(a). Many regions are visible, corresponding to the different morphologies observed at the front. Note that the cholesteric-nematic front disappears at small thicknesses ($d<14$ μm) since the sample is completely in the nematic state. In the diagram appears a gray zone corresponding to a gap of thicknesses d ranging between 33 μm and 36 μm. In practice, this region is unaccessible experimentally because making a 34.5 μm-thick sample is almost impossible (the thickness is known experimentally to about ± 1 μm).

We now describe in more detail the bifurcation diagram. It can be divided into six regions. In region I, the fingers (CF1) are perperpendicular to the front with their rounded tips at the front ("cells" regime). We recall that the rounded

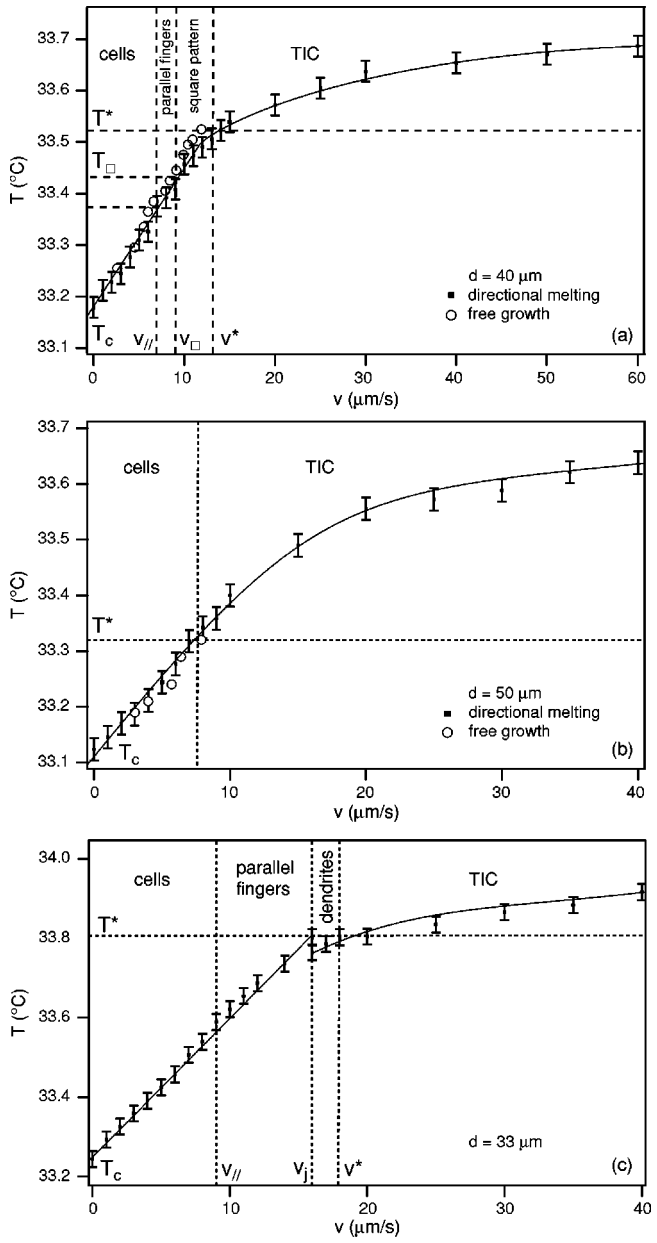

FIG. 7. (a) Front temperature vs velocity in a 40 μm-thick sample. The solid line is just a guide for the eyes; (b) front temperature vs velocity in a 50 μm-thick sample. The solid line is just a guide for the eyes. In both cases there is a good agreement between measurements performed in directional melting and in free growth; (c) front temperature vs velocity in a 33 μm-thick sample. The solid lines are just guides for eyes. Note the jump at the transition between the parallel fingers and the dendrites at v_j, analogous to the jump observed at the cell-to-dendrite transition in thin samples.

tip of a CF1 is more favorable energetically than its other pointed tip (which possesses, contrary to the rounded one, an internal zone twisted in opposite direction to the natural twist of the cholesteric phase, see Ref. [19]).

In region II, the fingers are still perpendicular to the font, but with their pointed tips at the front. This result is quite original as the system selects (in the dynamic regime, far from equilibrium) a front profile that is unfavorable energetically. In region III, the fingers are parallel to the front. In region IV, a square pattern forms just behind the front where a narrow band of TIC occurs.

Finally, the TIC solution fully develops at the front in regions V and VI. Note that in region V, the TIC forms continuously from the dendrites, whereas in region VI it forms from the cells: we thus expect that these two types of TIC are different, which we will prove in the following section.

In the experimental phase diagram of Fig. 9(a), these regions are separated by lines numbered from 1 to 5. These lines have been determined experimentally out of the gray region of the diagram. On the other hand, the question of connecting the lines in the gray region arises.

This question is addressed in the next section, where we discuss the topology of the different solutions. This question is of crucial importance, in particular for explaining the difference between the two types of TIC observed in regions V and VI. In particular, the exact nature of line 3 (dotted line) in the diagram will be clarified.

VI. TOPOLOGY OF THE DIFFERENT PATTERNS AND CONSTRUCTION OF THE FULL PHASE DIAGRAM

To complete the diagram in the gray region, we first note that lines 1 and 2 fix the limit of stability of the nematic phase. For this reason, they must join at some point, noted P in this part of the diagram [Fig. 9(b)]. The second problem is to determine how lines 3 and 5 prolong in this part of the diagram. To answer this question, let us first recall the topology of the TIC and of the fingers of the first kind.

We have known for a long time that all the textures observed in this experiment can be obtained from the homeotropic nematic phase by distorting continuously the director field. The most simple structure that allows the liquid crystal to express its chirality is the TIC. By definition, the TIC is a translationally invariant configuration in the plane of the sample, in which twist only occurs in the direction normal to the glass plates (z in the following). More precisely, the director **n** (which is a unit vector giving the average direction of the rodlike molecules) describes a cone tilted with respect to the normal to the plates when one follows a vertical line joining the lower plate to the upper one. The TIC can also be represented by a closed trajectory on the unit sphere S2. The principle of this representation is to associate a point on the sphere to a given orientation of the director. By convention, the north pole corresponds to the homeotropic nematic phase. In the TIC, the director changes orientation only in the direction perpendicular to the plates. Thus, the image on the sphere of a line perpendicular to the plates is a closed curve going through the north pole in $z=0$ (lower plate) and $z=d$ (upper plate). In the following, we introduce the **c** director that represents the unit vector parallel to the projection into the (x,y) plane of the director **n** at $z=d/2$. It is important to note that **c** and $-$**c** are not equivalent as they represent two different orientations of the TIC. That means that **c** behaves as a spin (by opposition to **n** for which **n** and $-$**n** are equivalent). Note that the same coordinate system (x,y,z) is em-

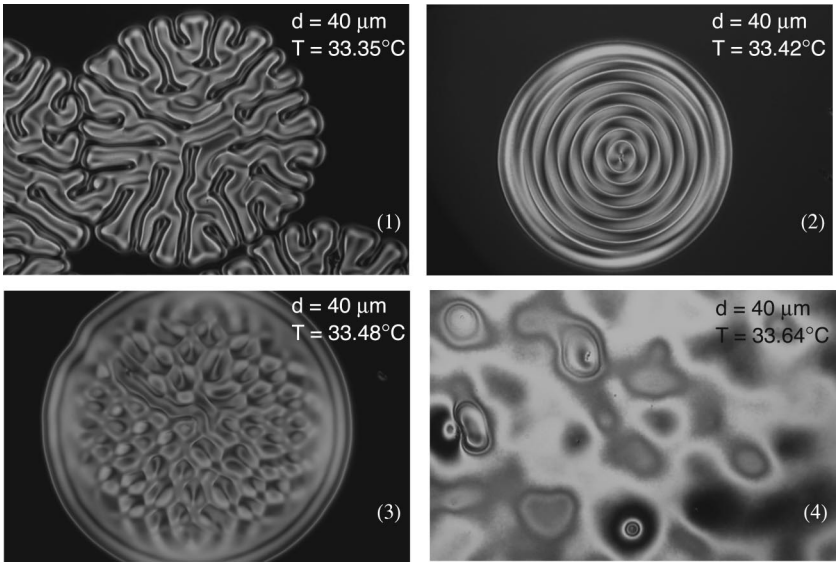

FIG. 8. Free growth of the cholesteric phase in a 40 μm-thick sample. At temperatures corresponding to photos (1–3) the nematic phase is metastable. At the temperature corresponding to photo (4), the nematic phase is unstable and develops a transient TIC structure (as in Fig. 7) after switching off the electric field.

ployed in real space and on the S2 sphere. In the following, we choose the y axis parallel to **c** and oriented in the same direction. The x axis is thus perpendicular to **c** [Fig. 10(a)]

The second important point is that the fingers of the first kind (CF1) can be obtained by periodically modulating the TIC (for further details see [19–26]. Energetical calculations show that this modulation appears favorably along a direction perpendicular to **c**, i.e., along the x axis with our conventions.

The third important point concerns the ends of a CF1. They are different (one is rounded, the other pointed) as there is no mirror symmetry in a cholesteric. In addition, the position of the two ends depends on the orientation of the **c** director, the rounded tip being on the side $x>0$, whereas the pointed one is on the side $x<0$ (for a right-handed cholesteric helix) [Fig. 10(b)]. The previous topological considerations allow us to precise the **c** orientation of the TIC which the fingers are coming from. Many cases must be considered.

In the cell regime observed at low velocity and all thicknesses (region I in the bifurcation diagram), the fingers are perpendicular to the front with their rounded tips at the front. That means that **c** is parallel to the front and directed towards the left if one chooses to orient the x axis towards the top of Fig. 10(c).

The situation is opposed in the dendritic regime (region II) observed in thin samples above some critical velocity. In this case, the pointed tips of the fingers form at the front. That means that the TIC, and thus the **c** director, have turned about 180° during the "cell-to-dendrite" transition (which, indeed, is discontinuous as shown on photos 3 and 4 of Fig. 1) [Fig. 10(d)]. On the other hand, the TIC keeps the same orientation in region V and in the dendritic regime, as the passage across line 1 (corresponding to the spinodal limit of the nematic phase) is continuous.

The orientation of the TIC in region VI is also the same as in region I. This is because the passage across line 2 at large thickness is continuous. In addition, the TIC which forms at the front in region VI relaxes towards fingers perpendicular to the front (in average), which indicates that the TIC has kept its initial orientation (in average). A consequence is that there should exist a line of separation between regions V and VI at large velocity, starting from point P in the phase diagram. This is the dotted line above point P in the bifurcation diagram of Fig. 9(b).

The situation is more delicate in region III, where the fingers are parallel to the front. If they were of the same nature as the usual CF1's, this would mean that the TIC has turned about ±90°. Such a transition should be discontinuous, which is not observed. On the contrary, we show that when crossing line 4, the rounded tips of the CF1's progressively merge together to give a smooth front, which subsequently modulates into fingers parallel to the front. This suggests that the orientation of the TIC has not changed. Another argument in favor of this thesis, is that we never observed domains of parallel fingers separated by bands of homeotropic nematic phase. Indeed, such a band should systematically form at the separation between two domains which would have rotated in opposite directions (+90° and −90°), knowing that two ends of the same type (rounded or pointed) cannot merge together [19]. For all these reasons, we conclude that the fingers parallel to the front are formed from a modulation of the initial TIC along x (instead of y). As a consequence, these fingers are less favorable energetically than the usual CF1's. This conclusion is reinforced by two supplementary observations: first, their optical contrast is different from that of usual fingers [see Figs. 6(2) and 8(2)] and, second, and more importantly, there exists a second well-defined interface behind the front (separating the parallel fingers from a zone filled with CF1's perpendicular to the front), which propagates at the same velocity as the front. This means that the CF1's are more favorable energetically than the parallel fingers, which are, thus, metastable. Finally, we think that the TIC from which the square lattice forms, has the same orientation as in region I. This is supported by the fact that the crossing of lines 5 and 2 is continuous.

As a consequence, line 3 in the experimental phase diagram [Fig. 9(a)] separates two regions in which the underlying **c** director is oriented in two opposite directions. This line is thus of the same nature as the dotted line starting from

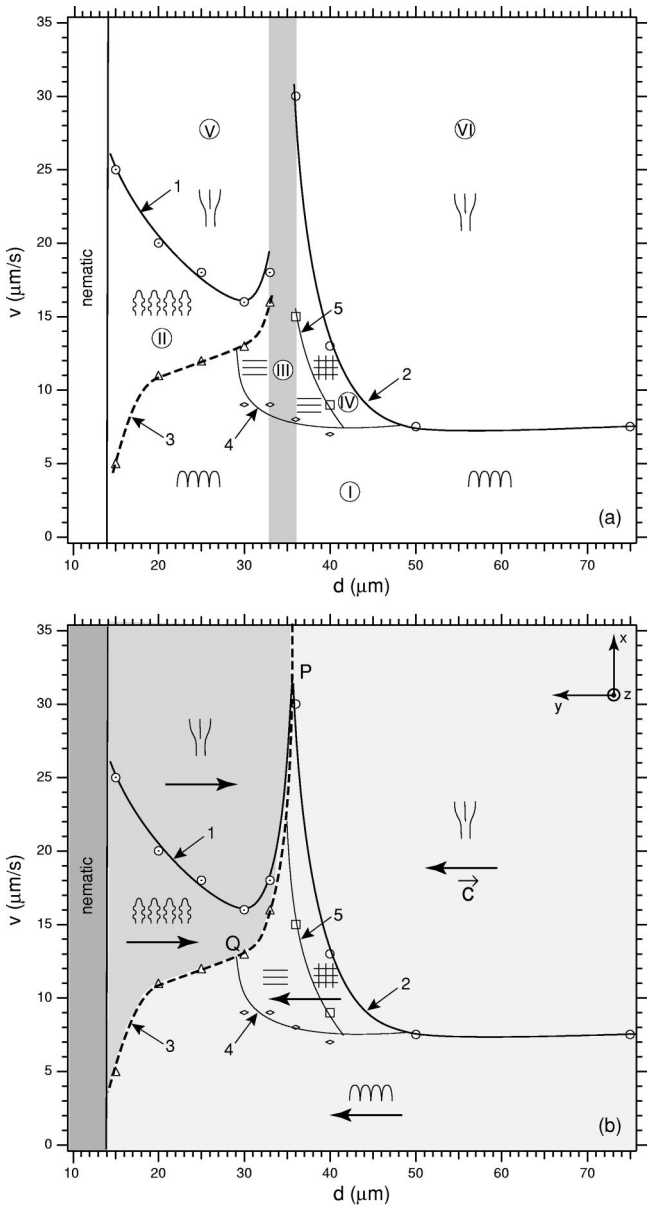

FIG. 9. (a) Bifurcation diagram observed in directional melting at the nematic-cholesteric front; (b) orientation of the **c** director (represented by an arrow) in the bifurcation diagram. The dotted line separates two large regions in which the **c** director has opposite directions.

point *P* and separating the regions V and VI. For that reason, it is natural to link together these two lines, which finally, form a single line [dotted line in Fig. 9(b)].

To summarize, we reported in the bifurcation diagram of Fig. 9(b) the orientation of the **c** director. Two principal regions must be distinguished, separated by the dotted line. The first one, on the left hand side of this line, contains regions II and V, previously defined. The second one (on the right hand side of this line) groups together regions I, III, IV, and VI.

The last question is how to continue line 5 in the gray region of the experimental phase diagram of Fig. 9(a). We can only say that this line must intersect the dotted line between points *P* and *Q* (where *Q* is the intersection point between lines 3 and 4).

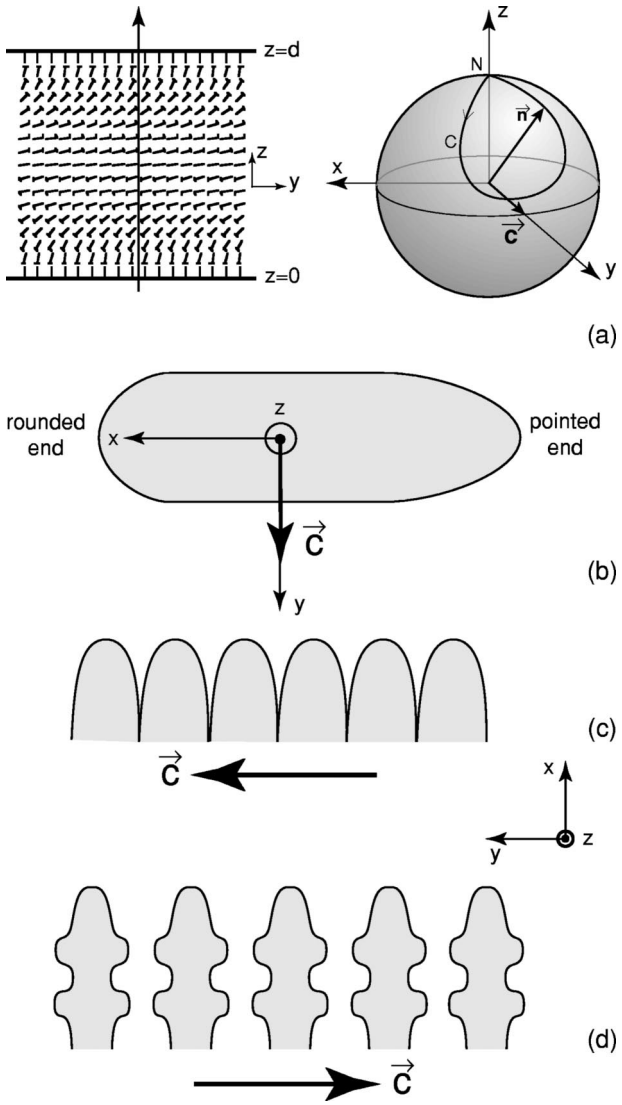

FIG. 10. (a) Representations in the real space and on the unit sphere S2 of the TIC; (b) orientation of the **c** director in a CF-1 segment with respect to the coordinate system (x,y,z); (c),(d) orientation of the **c** director in the cell regime (c) and in the dendritic regime (d).

In the following section, we discuss the origin of this reversal of the TIC.

VII. ABOUT THE ORIGIN OF THE REVERSAL OR OF THE NONREVERSAL OF THE TIC

In 1998, one of us (J.B.), in collaboration with C. Misbah, performed numerical simulations of the TIC-nematic front in directional melting. To simplify the calculations, simulations were performed assuming isotropic elasticity and were restricted to the TIC structure (knowing that this structure tends to modulate to give fingers). It was found that the TIC reverses at some finite velocity, similar to what we observe in thin samples, suggesting that the TIC-nematic transition is,

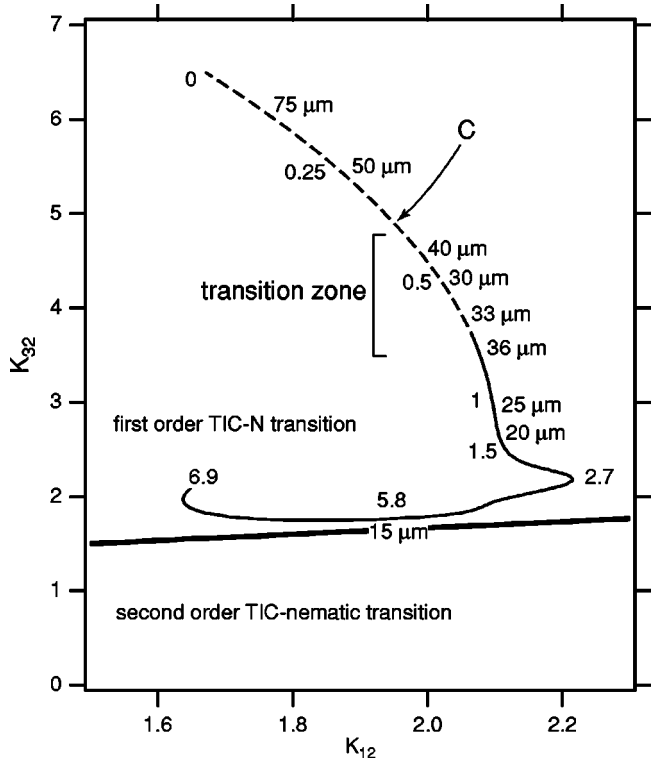

FIG. 11. Elastic parameter plane (K_{12},K_{12}). Below the straight line, the TIC-nematic transition is second order; above, it is first order. The curve C gives the values of the elastic parameters in 8CB as a function of the temperature T. The dotted part of curve C has been calculated from the extrapolation close to T_{NA} of the curve $K_3(T)$ shown in Fig. 12. The upper end of C corresponds to T_{NA} while the other corresponds to T_{NI}. A few values of $T-T_{NA}$ are indicated (in degrees Celsius) beside the curve (on the left). To each sample (whose the thickness is given in μm on the graph) corresponds a particular temperature T^* to which is associated a point on the curve. In thin samples the transition is weakly first order; in thick ones the transition is strongly first order.

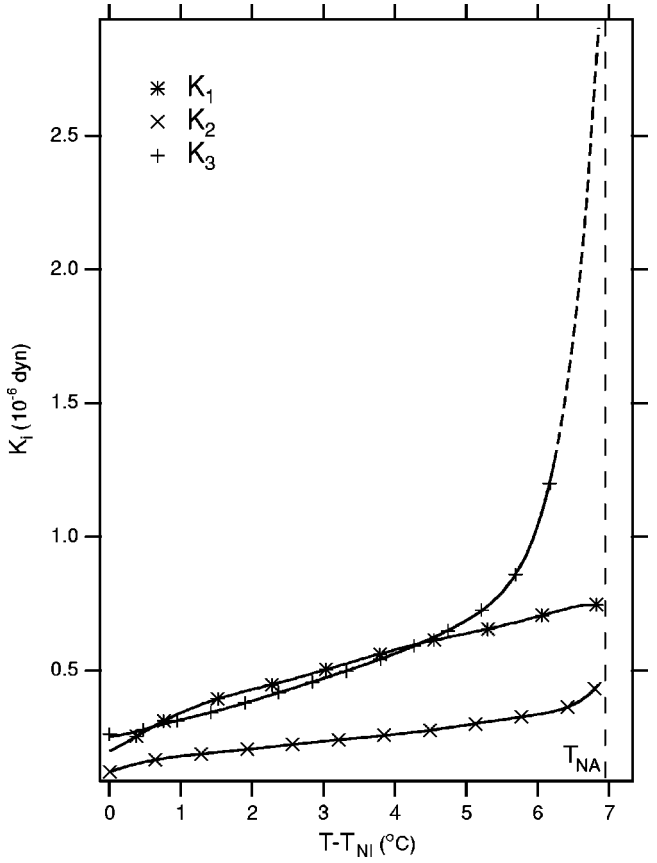

FIG. 12. Elastic constants as a function of the temperature in 8CB. Points are experimental (from Ref. [30]) and full lines are their best fits to a polynomial law. The dotted part of the curve $K_3(T)$ is obtained by extrapolation. It shows that K_3 diverges much rapidly than K_2 when $T\rightarrow T_{NA}$. This behavior is normal as the energy of the edge dislocations in the smectic phase is much larger than that of the screw dislocations. The fits have been used to calculate the characteristic curve C shown in Fig. 11.

if not second order, at least weakly first order in these samples. On the other hand, we do not observe the reversal of the TIC in thick samples, which suggests that the transition becomes too strongly first order in the latter (by admitting that the phenomenon is related to the importance of the first-order character of the transition).

To test this idea, we have measured in each sample the values of the coefficients of elastic anisotropy $K_{12}=K_1/K_2$ and $K_{32}=K_3/K_2$ at the temperature T^* (where K_1, K_2, and K_3 are, respectively, the splay, twist, and bend elastic constants [14]). We recall that the TIC develops at the front (and reverses in thin samples) at this particular temperature. In addition, we know that the nature of the TIC-nematic transition depends on the value of these two parameters. More precisely, the transition is second order below the line of equation

$$K_{32}=\frac{1}{3}K_{12}+1,$$

whereas it becomes first order above. This is shown in the graph of Fig. 11. Because the elastic constants are well known in 8CB [30] [except for K_3 very close to T_{NA}, where we extrapolated the curve $K_3(T)$, see Fig. 12], it is possible to calculate K_{12} and K_{32} for each temperature T ranging between T_{NI} (the transition temperature towards the isotropic phase) and T_{NA} (the transition temperature towards the smectic phase). Reporting these values as a function of temperature on the graph of Fig. 11 gives a curve C which lies entirely above the previous line, showing that the TIC-nematic transition is always first order in 8CB. One nevertheless observes that the nature of the transition depends on the temperature, as it is weakly first order between T_{NI} and $T_{NA}+1$ °C (typically), whereas it becomes strongly first order when the temperature approaches T_{NA}.

We can now estimate the strength of the first-order character of the transition in each sample when the TIC develops. Indeed, we have measured the front temperature T^* in each sample at the velocity v^* at which the TIC starts to grow, which allows us to locate the place of each sample on the curve C. This is shown in Fig. 11. As expected, we observe that the transition is weakly first order in thin samples in which the TIC reverses, whereas it is strongly first order in thick samples.

In conclusion, this analysis suggests that the TIC reversal, and more generally, the development of the different patterns observed in this experiment, is closely related to the elastic anisotropy. More precisely, the TIC reversal occurs when the anisotropy is small or, equivalently, when the transition is sufficiently weakly first order.

VIII. CONCLUSION

We have studied the patterns formed behind a moving cholesteric-nematic interface. We have established a much more complete bifurcation diagram than that given in Fig. 8 of Ref. [25]. A type of bifurcation has been discovered, which looks like a classical "cell-to-dentrite" transition in directional growth of a solid into its melt (in spite of the fact that the physics is completely different). This transition is discontinuous and has been associated to a π rotation of the underlying TIC. It is worth noting that this transition is specific for a chiral system in which mirror symmetries are absent.

The crossing through the spinodal limit of the nematic phase has also been identified by comparing the patterns observed in directional melting and in free growth. Finally, we emphasize that the reversal of the TIC only occurs in thin samples ($d \leqslant 35\ \mu$m), when the nematic-TIC transition is weakly first order. In contrast, the TIC does not change orientation in thick sample ($d \geqslant 35\ \mu$m) in which this transition becomes strongly first order. This is compatible with the numerical simulations one of us (J.B.) [26] performed assuming isotropic elasticity. In that case, the nematic-TIC transition is second order and the numerics shows the existence of a critical velocity above which the TIC rotates by π, as observed experimentally in thin samples.

Nevertheless, many questions are unsolved. In particular, it would be interesting to investigate the real structure of the square lattice and of the parallel fingers, two configurations that are clearly metastable and less favorable energetically than the usual fingers of the first kind (CF1). More generally, an important theoretical work remains to do for understanding the formation of these patterns. In particular, further numerical simulations including elastic anisotropy and using a full tensorial spatial-dependent order parameter, are necessary to determine in which region of the parameter plane (K_{12}, K_{32}) the TIC does no longer reverse.

ACKNOWLEDGMENT

We thank John Bechhoefer for a careful rereading of the manuscript and for very fruitful comments.

[1] W.A. Bentley and W.J. Humphrey, *Snow Crystals* (Dover, New York, 1962).
[2] J. Fineberg and V. Steinberg, Phys. Rev. Lett. **58**, 1332 (1987).
[3] G. Ahlers and D.S. Cannell, Phys. Rev. Lett. **50**, 1583 (1982).
[4] S.J. Di Bartolo and A.T. Dorsey, Phys. Rev. Lett. **77**, 4442 (1996).
[5] U. Ebert, W. van Saarloos and C. Caroli, Phys. Rev. E **55**, 1530 (1997).
[6] J.S. Langer, Rev. Mod. Phys. **52**, 1 (1980).
[7] T.R. Anantharaman and C. Suryanarayana, J. Mater. Sci. **6**, 1111 (1971).
[8] W.J. Boettinger and J.H. Perepezko, in *Fundamentals of Rapid Solidification*, edited by S.K. Das, B.H. Kear, and C.M. Adam (The Metallurgical Society of AIME, 1985), p. 21.
[9] L.S. Tuckerman and J. Bechhoefer, Phys. Rev. A **46**, 3178 (1992).
[10] W. van Saarloos, Phys. Rep. **301**, 9 (1998).
[11] V. Popa Nita and P. Oswald, Phys. Rev. E **66**, 066117 (2002).
[12] J. Bechhoefer, in *Pattern Formation in Liquid Crystals*, edited by A. Buka and L. Kramer (Springer, New York, 1996).
[13] K. Kassner, *Pattern Formation in Diffusion-Limited Crystal Growth* (World Scientific, Singapore, 1996), Chap. 9.
[14] P. Oswald and P. Pieranski, *Les Cristaux Liquides: Concepts et Propriétés Physiques Illustrés par des Expériences* (Gordon and Breach Science, Paris, 2000), Vol. 1; *ibid.* (CPI/Gordon and Breach Science, Paris, 2002), Vol. 2.
[15] A.J. Simon, J. Bechhoefer, and A. Libchaber, Phys. Rev. Lett. **61**, 2574 (1988).
[16] P. Oswald, J. Phys. II **1**, 571 (1991).
[17] H. Brehm, H. Finkelmann, and H. Stegemeyer, Ber. Bunsenges. Phys. Chem. **78**, 883 (1974).
[18] A. Stieb, J. Phys. (France) **41**, 961 (1980).
[19] P. Ribière and P. Oswald, J. Phys. (France) **51**, 1703 (1990).
[20] M.J. Press and A.S. Arrott, J. Phys. (France) **37**, 387 (1976).
[21] F. Lequeux, P. Oswald, and J. Bechhoefer, Phys. Rev. A **40**, 3974 (1989).
[22] T. Frisch, L. Gil, and J.-M. Gilli, Phys. Rev. E **48**, R4199 (1993).
[23] L. Gil, J. Phys. II **5**, 1819 (1995).
[24] P. Oswald, J. Baudry, and S. Pirkl, Phys. Rep. **337**, 67 (2000).
[25] P. Oswald, J. Bechhoefer, A. Libchaber, and F. Lequeux, Phys. Rev. A **36**, 5832 (1987).
[26] J. Baudry, Ph.D. thesis, Ecole Normale Supérieure de Lyon, 1999.
[27] P. Oswald, M. Moulin, P. Metz, J.C. Géminard, P. Sotta, and L. Sallen, J. Phys. III **3**, 1891 (1993).
[28] M.A. Anisimov, P.E. Cladis, E.E. Gorodetskii, D.A. Huse, V.E. Podneks, V.G. Taratuta, W. van Saarloos, and V.P. Voronov, Phys. Rev. A **41**, 6749 (1990).
[29] A. Yethiraj and J. Bechhoefer, Phys. Rev. Lett. **84**, 3642 (2000).
[30] N.V. Madhusudana and R. Pratibha Mol. Cryst. Liq. Cryst. **89**, 249 (1982).